Intermediate scalings for solv, nil, and $SL_2(\mathcal{R})$ black branes

Raúl E. Arias[1,*] and Ignacio Salazar Landea[2,3,†]
[1]SISSA, Via Bonomea 265, 34136 Trieste, Italy
[2]Centro Atómico Bariloche, 8400-S.C. de Bariloche, Río Negro, Argentina
[3]Instituto de Física de La Plata - CONICET C.C. 67, 1900 La Plata, Argentina

(Received 14 February 2019; published 31 May 2019)

In this work, we will study black brane solutions that are not translationally invariant in the spatial directions along which it extends. Instead, we require homogeneity, which still allows points along the spatial directions to be related to each other by symmetries. We find Einstein–Maxwell–anti-de Sitter black hole solutions of which the near-horizon geometry corresponds to solv (Bianchi $V1_{-1}$), nil (Bianchi II), or $SL_2(\mathcal{R})$ (Bianchi $VIII$). Interestingly, we observe that at intermediate temperatures our solutions have an scaling regime where different spacetime directions scale differently. We also compute the dc conductivities for these charged solutions and study how they scale in this intermediate regime.

DOI: 10.1103/PhysRevD.99.106015

I. INTRODUCTION

Quantum critical points and novel phases of matter with unconventional scalings are systems of which the degrees of freedom are believed to be in a strongly coupled regime. Then, holography is a good playground with many tools to study the dynamics of such systems. Moreover, there is an effort to classify phase structures, in particular, in the deep IR regime. The result of such efforts was the appearance of novel renormlization group (RG) flow geometries with intermediate scalings, which are useful to model the behavior of conformal field theories around quantum critical points. In this work, we will show new intermediate regimes in a class of Einstein-Maxwell theories that break translational invariance in a particular way that still preserves homogeneity.

In the context of the AdS/CFT approach to studying condensed matter physics, there has been significant recent interest in the construction of black hole solutions dual to conformal field theories (CFTs) deformed by operators that break translational invariance. This is because these systems allow momentum to dissipate, giving room to study more realistic transport properties. The breaking of translational invariance in holography is a complicated issue because typically this drives us to solve partial differential equations [1–3].

One way[1] to bypass this complication for theories in $d = 4$ dimensions is to generalize the generators of the translational symmetry to a Bianchi symmetry, in which they do not commute, and then exploit this new symmetry to get ordinary differential equations (ODEs) [9–14]. The Thurston geometrization conjecture gives a classification of geometries that are allowed to be the near-horizon limit of a black hole solution. There are just eight of such geometries [Euclidean space E_3, the 3-sphere S^3, the hyperbolic space H_3, the products $S_1 \times H_2$ and $S_1 \times S_2$, nil geometry, solv geometry, and lastly the universal cover $SL_2(\mathcal{R})$], and the remaining ones must be isometric to one of them. In the present work, we are going to elaborate on the direction of Ref. [13], and we will study black holes in which the horizons have Bianchi VI_{-1} (solv), Bianchi II (nil), or Bianchi $VIII$ [$SL_2(\mathcal{R})$] symmetries,

$$\begin{aligned} \text{solv}:\ & d\bar{s}^2 = e^{2kz}dx^2 + e^{-2kz}dy^2 + dz^2 \\ \text{nil}:\ & d\bar{s}^2 = dx^2 + dy^2 + (dz - kxdy)^2, \\ SL_2(\mathcal{R}):\ & d\bar{s}^2 = \frac{1}{k^2x^2}(dx^2 + dy^2) + \left(dz + \frac{dy}{kx}\right)^2, \end{aligned} \quad (1)$$

that we will generically write as

$$d\bar{s}^2 = \sum_{i=1}^{3} \omega_i^2. \quad (2)$$

For the solv geometry, $\omega_1 = e^{kz}dx$, $\omega_2 = e^{-kz}dy$, and $\omega_3 = dz$; for the nil solutions, $\omega_1 = dx$, $\omega_2 = dy$, and

*rarias@sissa.it
†peznacho@gmail.com

[1]Another powerful way to incorporate the effect of momentum dissipation and still work with ODEs is to effectively add the effect of inhomogeneities by giving a mass to the graviton [4–8].

$\omega_3 = dz - kxdy$; and for the $SL_2(\mathcal{R})$, we have $\omega_1 = dx/kx$, $\omega_2 = dy/kx$, and $\omega_3 = dz + dy/kx$.

In this setup, we will obtain solutions of the Einstein–Maxwell–anti-de Sitter (AdS) action in five dimensions,

$$\tilde{S} = \int d^5x\sqrt{-g}\left(R - 12 - \frac{1}{4}F_{\mu\nu}F^{\mu\nu}\right) + \tilde{S}_{\text{bdy}}, \quad (3)$$

where $\tilde{S}_{\text{bdy}}$ corresponds to some boundary action, solving the following equations of motion:

$$D_\mu F^{\mu\nu} = 0,$$
$$R_{\mu\nu} - \frac{1}{2}Rg_{\mu\nu} - 6g_{\mu\nu} = -\frac{1}{4}F_{\alpha\beta}F^{\alpha\beta}g_{\mu\nu} + F_{\mu\alpha}F^{\alpha}{}_{\nu}. \quad (4)$$

This action corresponds to the universal sector of many holographic models. In this context, we will build charged black hole solutions that will be dual to a finite temperature CFT at a finite chemical potential living in the spacetimes defined in (1).

This paper will elaborate on the solutions found in Ref. [13] by relaxing the ansatz for the metric. This will allow us to find solutions that are isotropic in the UV, giving a more natural framework for a holographic interpretation. We can now think of our solutions as the dual of a four-dimensional CFT deformed by placing the theory on a Bianchi manifold.

As recently reported in Refs. [2,15,16], breaking translational symmetry gives rise to new scalings at the IR or at intermediate scales. We will study these new scalings by constructing a family of black hole solutions by varying how badly the translational symmetry is broken. We will see that for neutral black holes new scalings will appear near the horizon of low reduced temperature T/k black holes. In these new scalings, different spatial coordinates will typically scale differently. When considering charged solutions, these new scalings become intermediate scalings, and our near-horizon solutions look like $\text{AdS}_2 \times$ Thurston.

Recently, it was argued [17] that many properties of strange metals could be explained from a simple scaling theory. Then, it is interesting to understand the mechanisms that make a theory develop nonconventional scalings. In this context, we show evidence that breaking the translational invariance on the universal sector of any theory with a gravity dual forces the theory to develop new scalings at low or intermediate temperatures.

Having the translational symmetry broken, the dual field theories will have finite dc transport coefficients. We can read such coefficients directly from the horizon metric following the method developed in Ref. [18]. We see that the dc conductivities also reflect the intermediate scalings at intermediate temperatures [19].

This paper is organized as follows. In each of the following sections, we show solutions to the Einstein-Maxwell equations with different Thurston geometry horizons. Then, we proceed to compute the thermoelectric transport coefficients in the direction in which the translational symmetry is broken. In Sec. II, we deal with solv horizons; in Sec. III, we deal with nil horizons; and in Sec. IV, we deal with $SL_2(\mathcal{R})$ horizons. Finally, in Sec. V, we summarize our results and discuss possible future directions.

II. SOLV BLACK HOLES WITH INTERMEDIATE SCALING

In this section, we will work with black holes with solv geometry horizons.

A. Solutions

We will consider the following ansatz for the gauge and metric fields:

$$A = A_t(r)dt,$$
$$ds^2 = -r^2f^2(r)g(r)dt^2 + \frac{1}{r^2g(r)}dr^2 + r^2h^2(r)(e^{2kz}dx^2 + e^{-2kz}dy^2) + \frac{r^2}{h^4(r)}dz^2. \quad (5)$$

Explicitly, the equations of motion (4) read

$$g' - \frac{4}{r} + \frac{2k^2h^4}{3r^3} + \frac{A_t'^2}{3rf^2} + \left(\frac{4}{r} + \frac{2rh'^2}{h^2}\right)g = 0,$$
$$3r^4fh'' + \left(12 + 3g - \frac{A_t'^2}{g^2}\right)r^3h' - 2k^2(h^5 + rh^4h') - \frac{3r^4gh'^2}{h} = 0,$$
$$h^2f' - 2rfh'^2 = 0,$$
$$A_t'' + \left(\frac{3}{r} - \frac{f'}{f}\right)A_t' = 0, \quad (6)$$

with primes denoting radial derivative $' = \partial_r$ and where we drop the r dependence of the metric and gauge functions.

We will look for black hole solutions to these equations by integrating out the fields from the near horizon,

$$A_t(r) \simeq a_{t_1}(r-r_h) - \frac{a_{t_1}(12f_0^2h_0^4k^2r_h^2(a_{t_1}^2-12f_0^2)+3r_h^4(a_{t_1}^2-12f_0^2)^2+4f_0^4h_0^8k^4)}{2r_h(r_h^2(a_{t_1}^2-12f_0^2)+2f_0^2h_0^4k^2)^2}(r-r_h)^2+\ldots,$$
$$f(r) \simeq f_0 + \frac{8f_0^5h_0^8k^4}{r_h(r_h^2(a_{t_1}^2-12f_0^2)+2f_0^2h_0^4k^2)^2}(r-r_h)+\ldots,$$
$$g(r) \simeq \frac{r_h^2(12-\frac{a_{t_1}^2}{f_0^2})-2h_0^4k^2}{3r_h^3}(r-r_h)+\ldots,$$
$$h(r) \simeq h_0 - \frac{2f_0^2h_0^5k^2}{r_h^3(a_{t_1}^2-12f_0^2)+2f_0^2h_0^4k^2r_h}(r-r_h)+\ldots, \tag{7}$$

towards the boundary

$$g(r) \approx 1 - \frac{h_\infty^4k^2}{3r^2} + \frac{g_4^\infty}{r^4} + \frac{2h_\infty^8k^4\log r}{r^4}+\ldots,$$
$$h(r) \approx h_\infty - \frac{h_\infty^5k^2}{6r^2} + \frac{h_4^\infty}{r^4} + \frac{h_\infty^9k^4\log r}{9r^4}+\ldots,$$
$$f(r) \approx f_\infty - \frac{f_\infty h_\infty^8k^4}{r^4}+\ldots,$$
$$A_t(r) \approx \mu + \frac{\rho}{r^2} - \frac{2\rho f_\infty h_\infty^8k^4}{108f_\infty r^6}+\ldots. \tag{8}$$

The parameters a_{t_1}, f_0, and h_0 are the independent coefficients of the functions expanded around the horizon, and h_∞, h_4^∞, g_∞, g_4^∞, and f_∞ are the corresponding ones when the expansion is around the UV. These boundary conditions imply that our black hole solutions have the same scaling for the metric (towards the boundary) in all the directions, which is an important difference with respect to previous works [11–13]. The log terms are associated with an anomalous scaling of physical quantities due to the conformal anomaly. As expected, they go to zero when considering $k \to 0$.

The thermodynamics of the black hole are given by its temperature T and entropy density s,

$$T = \frac{1}{4\pi}\left(\frac{g_{tt}'}{\sqrt{g_{rr}g_{tt}}}\right)_{r=r_h} = \frac{\left(\frac{a_{t_1}^2}{3f_0}-4f_0\right)r_h + \frac{2f_0h_0^4k^2}{3r_h}}{4\pi},$$
$$s = 2\pi A_h = 2\pi r_h^3, \tag{9}$$

with A_h denoting the area of the black hole horizon. We find a family of solutions that we characterize by the dimensionless parameters T/k and μ/k.

For simplicity, let us begin by studying solutions with $\mu = 0$, corresponding to neutral black holes. Integrating the equations of motion, we find a family of solutions with different T/k. In the right panel of Fig. 1, we show how the entropy of the corresponding solutions scales with respect to the temperature. As we can see, for high enough temperatures, we see the expected CFT_4 related scaling $s/k^3 \sim (T/k)^3$. On the other hand, for low enough temperatures, we find a new scaling, $s/k^3 \sim (T/k)^2$. To better understand the nature of this new scaling, we must study in detail the behavior of the metric fields.

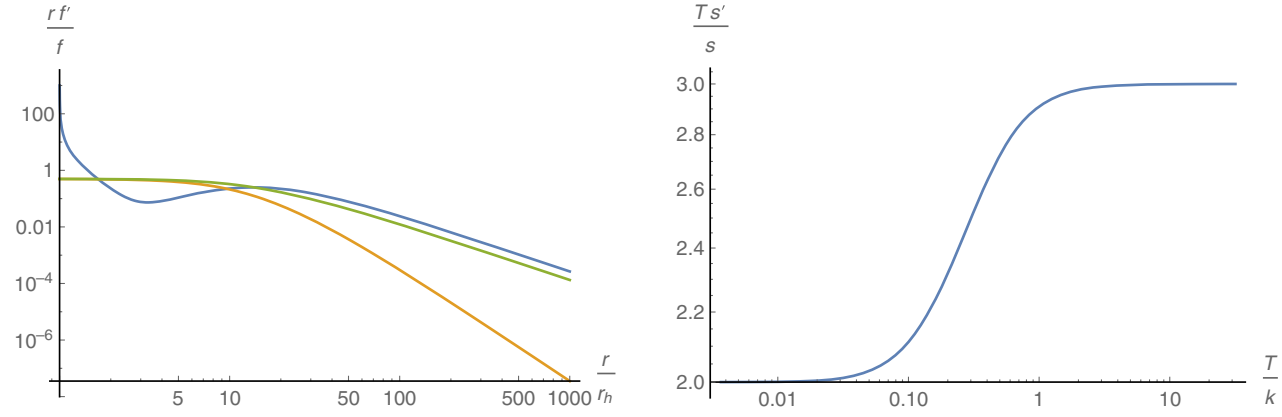

FIG. 1. Left: Typical profile for $f(r)$ (blue), $g(r)$ (orange), and $h(r)$ (green). The combination rf'/f, where f corresponds to any of the aforementioned functions, was chosen to make manifest the emergence of new scalings towards the IR. The plot corresponds to a solution with $T/k = 0.00367$ and $\mu/k = 0$. Right: Ts'/s as a function of the reduced temperature T/k.

In the left panel of Fig. 1, we show a typical plot for the metric fields as a function of the radial coordinate, when considering a solution with low enough T/k. From the numerics, we extract that the fields g and h of the metric get a new scaling at small r/r_h, such that $g \sim h \sim r^{1/2}$. Plugging this again into the metric, one can extract the following scalings:

$$t \to \lambda t, \qquad x \to \lambda x, \qquad y \to \lambda y, \qquad z \to z. \tag{10}$$

This means that we have anisotropic scalings, but these are not of the standard Lifshitz type, since it is one of the spatial directions that scales differently to the other spatial directions.

It seems tempting to associate the intermediate scaling geometry with

$$A = 0,$$
$$\frac{4}{3}ds^2 = -r^2dt^2 + \frac{1}{r^2}dr^2 + r^2(e^{2kz}dx^2 + e^{-2kz}dy^2) + \frac{2k^2}{3}dz^2. \tag{11}$$

This is an exact solution to the Einstein-Maxwell equations of motion. These exact solutions were previously studied in Refs. [11–13]. Here, we show how these solutions emerge naturally in the IR regime when studying black hole solutions with solv geometry horizons that are asymptotically isotropic.

If we now turn to charged black hole solutions, the IR scaling becomes an intermediate scaling, and the geometry flows into $AdS_2 \times$ solv in the deep near-horizon regime, as expected for a charged black hole. In Fig. 2, we show typical profiles for the fields and the scaling of the entropy for a family of solutions with fixed $\mu/k = 0.01$.

It is important to notice that the value of the chemical potential in units of k must be small enough to have intermediate scaling solutions. If it is not, then the $AdS_2 \times$ solv geometry will appear at larger values of the radius and will ruin the intermediate scaling. In other words, we need μ/k small enough so that the intermediate scaling has enough room to appear. The same argument will hold for the nil and $SL_2(\mathcal{R})$ cases of the next sections.

B. Finite conductivities from solv horizons

Consider a system at equilibrium at finite chemical potential and temperature. Adding a small electric field E_i or thermal gradient $\nabla_i T$ will induce an electric current J^i and a heat current $Q^i = T^{ti} - \mu J^i$, where T^{ij} is the stress tensor of the dual field theory. At linearized order, the response is controlled by the Ohm/Fourier law

$$\begin{pmatrix} J \\ Q \end{pmatrix} = \begin{pmatrix} \sigma & \alpha T \\ \bar{\alpha} T & \bar{\kappa} T \end{pmatrix} \begin{pmatrix} E \\ -\nabla T/T \end{pmatrix}, \tag{12}$$

defining the electric conductivity σ, the thermoelectric conductivities α and $\bar{\alpha}$, and the thermal conductivity $\bar{\kappa}$.

Systems with translation invariance and finite charge density have an infinite dc conductivity. Nonetheless, in the directions in which the translation invariance is broken, we expect a finite dc conductivity. That will be the z direction in our solv geometry charged black holes or the x direction in our nil geometry and $SL_2(\mathcal{R})$ charged black holes. We will read then the coefficients of the matrix (12) from horizon data, following the method developed in Ref. [18].

The holographic dictionary gives us the expressions for the electric and heat current in the dual field theory [20,21]

$$J = \sqrt{-g}F^{ri},$$
$$Q = \sqrt{-g}G^{ri} + JA_t, \tag{13}$$

where the tensor $G^{\mu\nu}$ reads

$$G^{\mu\nu} = \nabla^\mu k^\nu + \frac{1}{3}k^{[\mu}F^{\nu]\sigma}A_\sigma, \tag{14}$$

$k = \partial_t$, and the index i denotes the direction in which the electric field is applied.

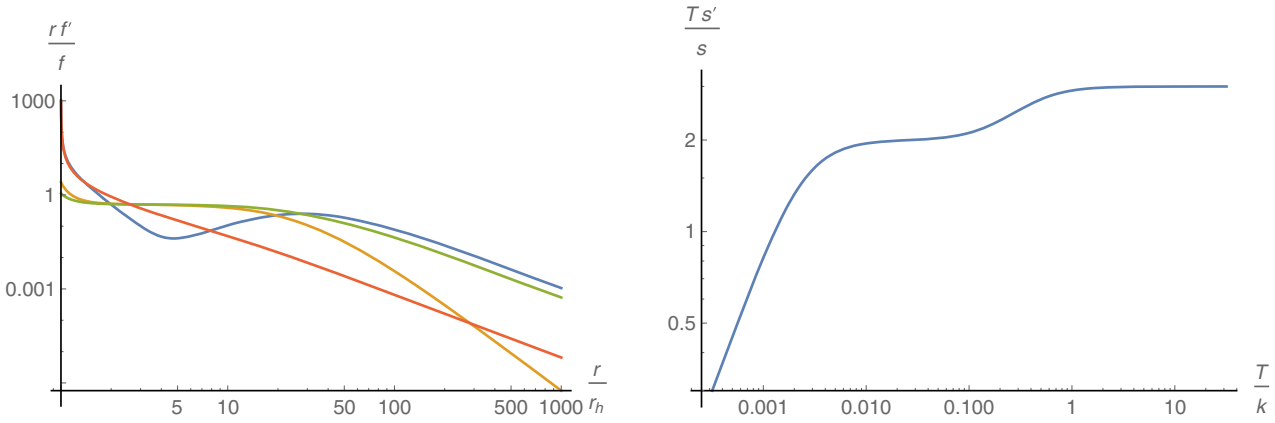

FIG. 2. Left: Typical profile for $f(r)$ (blue), $g(r)$ (orange), $h(r)$ (green), and $A_t(r)$ (red). The combination rf'/f, where f corresponds to any of the aforementioned functions, was chosen to make manifest the emergence of new scalings towards the IR. The plot corresponds to a solution with $T/k = 0.0003185$ and $\mu/k = 0.01$. Right: Ts'/s as a function of the reduced temperature T/k.

1. Computing σ and $\bar{\alpha}$

Let us begin with the computation of the electric conductivity and one of the thermoelectric conductivities $\bar{\alpha}$. To do that, we will study the linear response under the fluctuations of the metric and gauge field

$$\begin{aligned}\delta A &= (-Et + \delta a_z(r))dz \\ \delta ds^2 &= h_{tz}(r)dtdz + h_{rz}(r)drdz,\end{aligned} \tag{15}$$

where the constant E is the applied (dc) electric field. From the Maxwell equations, we obtain the following expression for the electric current J:

$$J = \frac{rh^4(h_{tz}A_t' + 2f^2r^2ga_z')}{2f}. \tag{16}$$

To have clean expressions, we will not write the r dependence of the functions. It is easy to check that the equation of motion for δa_z is equivalent to $\partial_r J = 0$. This allows us to evaluate the current at any value of the radial coordinate; in particular, we want to express the transport coefficients as function of IR data, i.e., the position of the horizon of the black hole.

Using the Einstein equations, we obtain that the heat current can be written as

$$Q = \frac{rh^4(2A_th_{tz}A_t' + rf^2(g(4rA_ta_z' + rh_{tz}' - 2h_{tz}) - rh_{tz}g') - 2r^2fgh_{tz}f')}{4f}. \tag{17}$$

Again, we can see that $\partial_r Q = 0$, and then we can evaluate it on $r = r_h$. The remaining Einstein equation is

$$h_{rz} = -\frac{r^2EA_t'}{k^2f^2gh^4}. \tag{18}$$

For a free-falling observer, the horizon of a black hole is a regular place; then, the electromagnetic field must be regular there. Using Eddington-Finkelstein coordinates $dv = dt + \sqrt{\frac{g_{rr}}{g_{tt}}}dr$ and asking for regularity of the fluctuations at $r = r_h$, we can obtain the near-horizon behavior of h_{tz} and δa_z. Using the expansions (7) and the near-horizon limit of (18), we can express the electric current and the heat kernel as function of IR data as

$$\begin{aligned}J &= \frac{1}{2}r_h^3E\left(-2h_0^4 + \frac{a_{t_1}^2}{f_0^2k^2}\right), \\ Q &= -\frac{a_{t_1}r_h^2E(r_h^2(12 - \frac{a_{t_1}^2}{f_0^2}) - 2h_0^4k^2)}{12k^2}.\end{aligned} \tag{19}$$

From this, we can compute the conductivities σ and $\bar{\alpha}$,

$$\begin{aligned}\sigma &= \frac{\partial J}{\partial E} = \frac{1}{2}r_h^3\left(2h_0^4 + \frac{a_{t_1}^2}{f_0^2k^2}\right), \\ \bar{\alpha} &= \frac{1}{T}\frac{\partial Q}{\partial E} = \frac{\pi a_{t_1}r_h^3}{f_0k^2}.\end{aligned} \tag{20}$$

In Fig. 3, we show these conductivities for the family of solutions presented in Fig. 2. From the plot, we see that at high temperatures we have $\sigma/k \sim \bar{\alpha} \sim T/k$, which agrees with the expectations for a CFT_4. In the low-temperature regime, we have $\sigma \approx (T/k)^{0.14}$ and $\bar{\alpha} \approx 0.005$. Interestingly, for intermediate temperatures, we see that the conductivities develop a power law scaling, in agreement with the intermediate scaling discussed previously. To be precise, we find that for intermediate temperatures we have $\sigma/k \sim (T/k)^{1.88}$ and $\bar{\alpha} \sim (T/k)^{0.39}$.

2. Computing α and $\bar{\kappa}$

Now, we move to compute the remaining conductivities, the thermoelectric coefficient α, and the thermal conductivity $\bar{\kappa}$. To do that, we implement the following perturbations in the metric and gauge field:

$$\begin{aligned}\delta A &= (-t\delta f_1(r) + \delta a_x(r))dx, \\ \delta ds^2 &= (-t\delta f(r) + h_{tx}(r))dxdt + h_{rx}(r)dxdr.\end{aligned} \tag{21}$$

Following as in the previous section, we obtain expressions for J and Q that do not depend on the radial direction

$$\begin{aligned}J &= \frac{rh^4(h_{tx}A_t' + t\delta fA_t' + 2r^2f^2g(a_x' - t\delta f_1'))}{2f}, \\ Q &= -JA_t - \frac{1}{4}r^5h^4f^3g^2\left[\left(\frac{h_{tx}}{r^2f^2g}\right)' + t\left(\frac{\delta f}{r^2f^2g}\right)'\right].\end{aligned} \tag{22}$$

We can erase the temporal dependence, fixing

$$\begin{aligned}\delta f_1(r) &= E + \zeta A_t, \\ \delta f(r) &= 2\zeta r^2f^2g.\end{aligned} \tag{23}$$

The remaining Einstein equation reads

$$\delta h_{rx} = \frac{r(2\zeta f^2(3r^2gh'^2 + 6rghh' + 6(r^2 - g)h^2 - k^2h^6) - rh^2A_t'(\zeta rA_t' + 6\zeta A_t + 6E))}{6k^2f^2gh^6}. \tag{24}$$

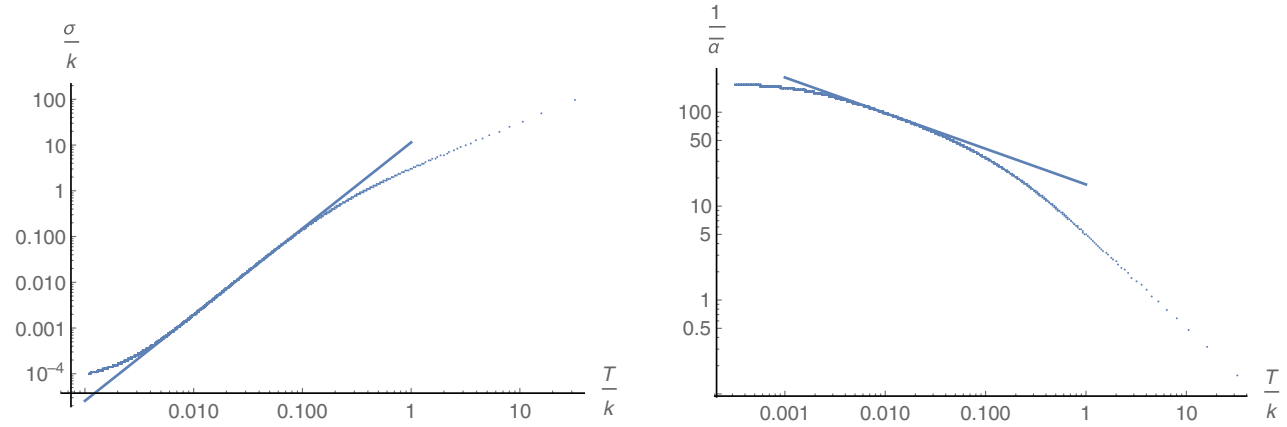

FIG. 3. Plot for the conductivities σ and $\bar{\alpha}$ as functions of the reduced temperature T/k for a family of solutions with fixed $\mu/k = 0.01$. The straight lines correspond to fits in the intermediate scaling regime.

Using the Eddington-Filkenstein coordinates and the expansions (7) and asking regularity at the horizon, we can express J and Q as

$$J = \frac{1}{12} r_h^2 \left(\frac{a_{t_1} r_h (\zeta r_h (a_{t_1}^2 - 12 f_0^2) + 6 a_{t_1} E)}{f_0^2 k^2} + 2 h_0^4 (a_{t_1} \zeta + 6 r_h E) \right),$$
$$Q = \frac{r_h (r_h^2 (12 - \frac{a_{t_1}^2}{f_0^2}) - 2 h_0^4 k^2)(\zeta r_h^2 (a_{t_1}^2 - 12 f_0^2) + 6 a_{t_1} r_h E + 2 \zeta f_0^2 h_0^4 k^2)}{72 k^2}. \tag{25}$$

The transport coefficients then read

$$\alpha = \frac{\pi a_{t_1} r_h^3}{f_0 k^2},$$
$$\bar{\kappa} = -\frac{\pi r_h^2 (a_{t_1}^2 r_h^2 + 2 f_0^2 (h_0^4 k^2 - 6 r_h^2))}{6 f_0 k^2}. \tag{26}$$

We see that $\alpha = \bar{\alpha}$, as it should be, because the transport matrix is symmetric. This is a nontrivial check on our computations. A quantity of interest is the thermal conductivity at zero electric current, which reads

$$\kappa = \bar{\kappa} - \frac{\alpha \bar{\alpha} T}{\sigma} = -\frac{\pi f_0 h_0^4 r_h^2 (a_{t_1}^2 r_h^2 + 2 f_0^2 (h_0^4 k^2 - 6 r_h^2))}{3 (a_{t_1}^2 + 2 f_0^2 h_0^4 k^2)}. \tag{27}$$

In Fig. 4, we plot the thermal conductivities $\bar{\kappa}$ and κ for a family of black holes at fixed chemical potential $\mu/k = 0.01$. For large temperatures, we see that both these quantities scale as $\bar{\kappa} \sim \kappa \sim (T/k)^2$. For low temperatures, on the other hand, we have that $\bar{\kappa} \sim T/k$, while $\kappa \sim (T/k)^{3/2}$. In the intermediate regime, we find that $\bar{\kappa} \sim \kappa \sim (T/k)^{1.66}$.

Dramatic differences between these two conductivities are indicators of the breakdown of the quasiparticle picture [22]. Moreover, in systems that behave as Fermi liquids, the ratio $\kappa/(\sigma T)$ is constant and has a value of $\pi^2/(3(k_B/e)^2)$, with e being the electric charge and k_B being the Boltzmann constant. Deviations from this constant value tell us that we are in a strong coupling regime. As we can see, κ and $\bar{\kappa}$ scale differently in the low-temperature limit but get closer together as we increase the temperature.

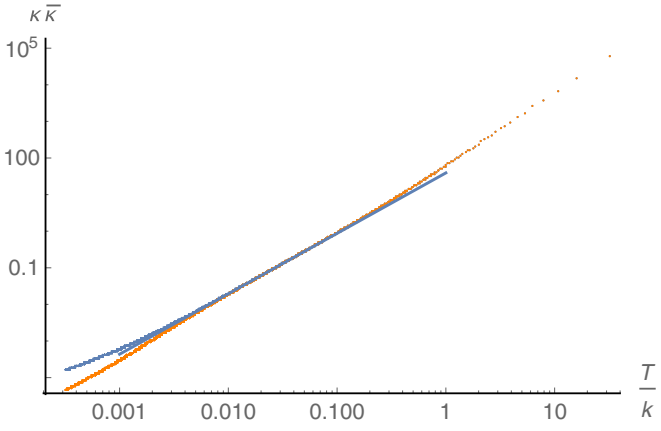

FIG. 4. Plot for the conductivities $\bar{\kappa}$ (blue) and κ (orange) as functions of the reduced temperature T/k for a family of solutions with fixed $\mu/k = 0.01$. The straight lines correspond to fits in the intermediate scaling regime.

III. NIL BLACK HOLES WITH INTERMEDIATE SCALING

We will now consider charged black holes solutions with nil horizon geometry.

A. Solutions

Let us then consider the ansatz

$$A = A_t(r)dt,$$
$$ds^2 = -r^2 g(r) f(r)^2 dt^2 + \frac{1}{r^2 g(r)} dr^2 + r^2 h^2(r)(dx^2 + dy^2) + \frac{r^2}{h^4(r)}(dz - kx dy)^2, \tag{28}$$

for which the equations of motion read

$$\frac{2r^2(12 - \frac{A_t'^2}{f^2}) - \frac{k^2}{h^8}}{6r^3} - g' + g\left(-\frac{2rh'^2}{h^2} - \frac{4}{r}\right) = 0,$$
$$h'' - \frac{\frac{2r^3 h'(A_t'(r)^2 - 3f^2(g+4))}{f^2} + \frac{6r^4 g h'^2}{h} + \frac{k^2 r h'}{h^8} - \frac{2k^2}{h'}}{6r^4 g} = 0,$$
$$f' - \frac{2rfh'^2}{h^2} = 0,$$
$$A_t'' - \frac{A_t'(rf' - 3f)}{rf} = 0. \tag{29}$$

We will look for black hole solutions to these equations by integrating out the fields from the near horizon,

$$A_t(r) \simeq a_{t_1}(r - r_h) - \frac{a_{t_1}(12h_0^{16} r_h^4 (a_{t_1}^2 - 12f_0^2)^2 + 12 f_0^2 h_0^8 k^2 r_h^2 (a_{t_1}^2 - 12 f_0^2) - 5 f_0^4 k^4)}{2r_h(2h_0^8 r_h^2 (a_{t_1}^2 - 12 f_0^2) + f_0^2 k^2)^2}(r - r_h)^2 + \ldots,$$
$$f(r) \simeq f_0 + \frac{8 f_0^5 k^4}{r_h(2h_0^8 r_h^2 (a_{t_1}^2 - 12 f_0^2) + f_0^2 k^2)^2}(r - r_h) + \ldots,$$
$$g(r) \simeq \frac{r_h^2(24 - \frac{2a_{t_1}^2}{f_0^2}) - \frac{k^2}{h_0^8}}{6r_h^3}(r - r_h) + \ldots,$$
$$h(r) \simeq h_0 + \frac{2 f_0^2 h_0 k^2}{2h_0^8 r_h^3 (a_{t_1}^2 - 12 f_0^2) + f_0^2 k^2 r_h}(r - r_h) + \ldots, \tag{30}$$

towards the boundary

$$A_t(r) \simeq \mu + \frac{\rho}{r^2} - \frac{\rho k^4}{216 h_\infty^{16} r^6} + \ldots,$$
$$f(r) \simeq f_\infty - \frac{f_\infty k^4}{72 h_\infty^{16} r^4} + \ldots,$$
$$g(r) \simeq 1 - \frac{k^2}{12 h_\infty^8 r^2} + \frac{g_4^\infty}{r^4} + \frac{k^4 \log r}{18 h_\infty^{16} r^4} + \ldots,$$
$$h(r) \simeq h_\infty + \frac{k^2}{12 h_\infty^7 r^2} + \frac{h_4^\infty}{r^4} - \frac{k^4 \log r}{18 h_\infty^{15} r^4} + \ldots, \tag{31}$$

where we will shoot for finding solutions with $f_\infty = h_\infty = 1$. Again, this boundary condition implies that our black hole solutions have the same scaling for the metric (in all the directions) when we move towards the boundary. The thermodynamics of the black hole are given by

$$T = \frac{\frac{a_{t_1}^2 r_h}{3 f_0} + \frac{f_0 k^2}{6 h_0^8 r_h} - 4 f_0 r_h}{4\pi}, \tag{32}$$
$$s = 2\pi A_h = 2\pi r_h^3. \tag{33}$$

As in the previous section, we will characterize the family of solutions with the dimensionless parameters T/k and μ/k.

For simplicity, let us begin by studying solutions with $\mu = 0$, corresponding to neutral black holes. Integrating the equations of motion, we find a family of solutions with different T/k. On the right panel of Fig. 5, we show how the entropy of the corresponding solutions scales with respect to the temperature. Again, for high enough temperatures, we see the expected CFT_4 related scaling $s/k^3 \sim (T/k)^3$. On the other hand, for low enough temperatures, we find a new scaling, $s/k^3 \sim (T/k)^{30/11}$. To better understand the nature of this new scaling, we must study in detail the behavior of the metric fields.

On the left-hand side of Fig. 5, we show the scalings related to the profiles of the metric functions for a low T/k solution. Far away from the horizon, we see that the metric behaves as demanded in (31). On the other hand, we find that near the horizon the metric functions behave differently, $h \sim r^{-1/4}$ and $g \sim r^{1/8}$. Plugging these scalings back into the metric gives quite a peculiar scaling,

$$t \to \lambda^{11/8} t, \quad \omega_1 \to \lambda \omega_1, \quad \omega_2 \to \lambda \omega_2, \quad \omega_3 \to \lambda^{3/2} \omega_3, \tag{34}$$

which gives the correct scaling for the entropy as a function of the temperature [23]. Unfortunately, we do not know of

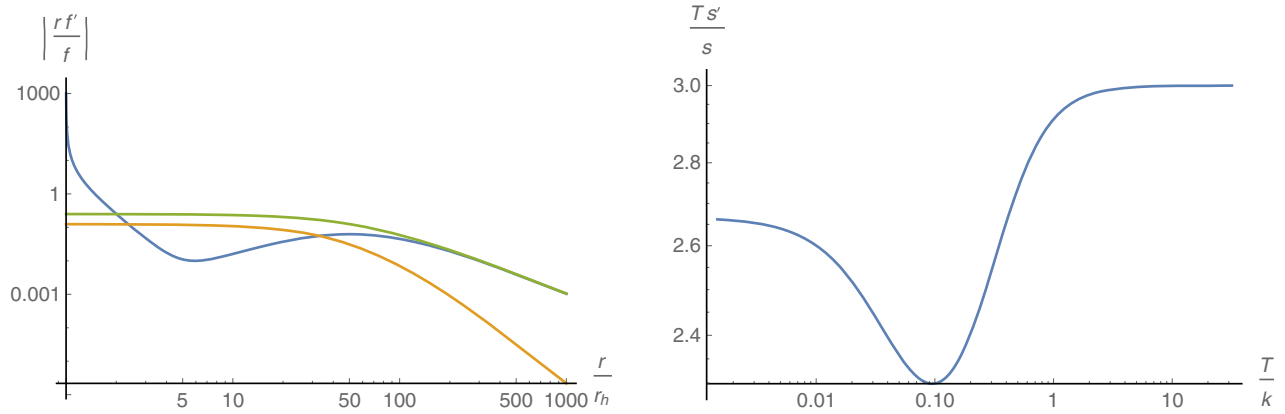

FIG. 5. Left: Typical profile for $f(r)$ (blue), $g(r)$ (orange), and $h(r)$ (green). The combination rf'/f, where f corresponds to any of the aforementioned functions, was chosen to make manifest the emergence of new scalings towards the IR. The plot corresponds to a solution with $T/k = 0.00147$ and $\mu/k = 0$. Right: Ts'/s as a function of the reduced temperature T/k.

a deformed theory from which we can extract exactly this kind of solutions.

Let us now study the charged solutions. In Fig. 6, we show typical profiles for the fields and the scaling of the entropy for a family of solutions with fixed $\mu/k = 0.01$. Again, the neutral IR scaling becomes an intermediate scaling, and the charged solutions flow to $AdS_2 \times nil$ at the IR.

B. Finite conductivities from nil horizons

In this subsection, we will compute the transport coefficients for this Einstein-Maxwell solutions and show how they scale along the RG flow. To express the transport coefficients as functions of horizon data, we must follow the same steps we used in the previous section; so, we are not going to repeat the procedure, and we are just going to highlight the final results.

In this case, the fluctuations must be along the x direction,

$$\begin{aligned}\delta A &= (-Et + \delta a_x(r))dx,\\ \delta ds^2 &= h_{tx}(r)dtdx + h_{rx}(r)drdx,\end{aligned} \tag{35}$$

with the constant E being the applied (dc) electric field. From the Einstein-Maxwell equations, we compute the conserved current and charge J and Q, and the remaining equation for h_{rx} reads

$$h_{rx} = -\frac{4Eh^8 A_t'}{k^2 f^2 g}. \tag{36}$$

Using the near-horizon data and asking for regularity, we obtain

$$\begin{aligned}J &= \frac{2a_{t_1}^2 h_0^6 r_h^3 E}{f_0^2 k^2} - \frac{r_h E}{h_0^2},\\ Q &= -\frac{a_{t_1} h_0^6 r_h^2 E\left(r_h^2\left(24 - \frac{2a_{t_1}^2}{f_0^2}\right) - \frac{k^2}{h_0^8}\right)}{6k^2},\end{aligned} \tag{37}$$

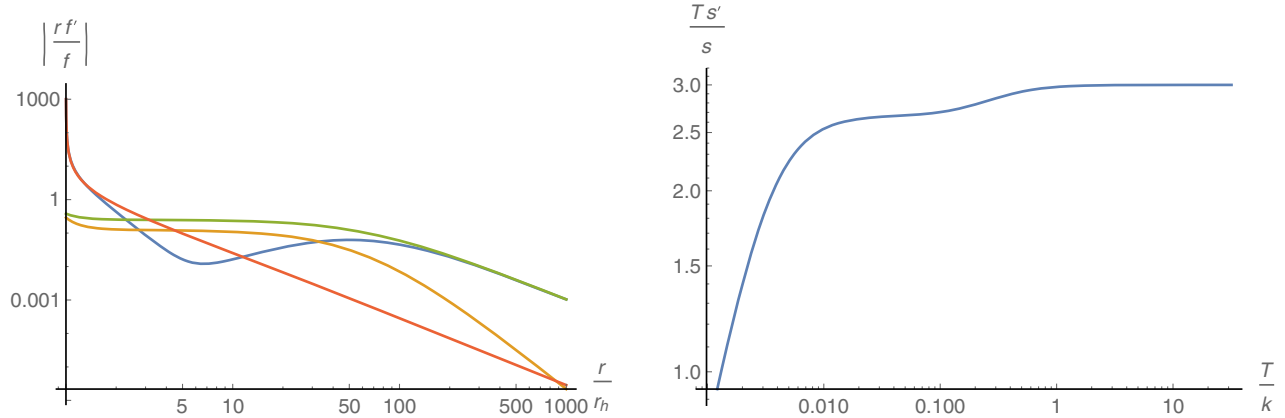

FIG. 6. Left: Typical profile for $f(r)$ (blue), $g(r)$ (orange), $h(r)$ (green), and $A_t(r)$ (red). The combination rf'/f, where f corresponds to any of the aforementioned functions, was chosen to make manifest the emergence of new scalings towards the IR. The plot corresponds to a solution with $T/k = 0.0003185$ and $\mu/k = 0.01$. Right: Ts'/s as a function of the reduced temperature T/k.

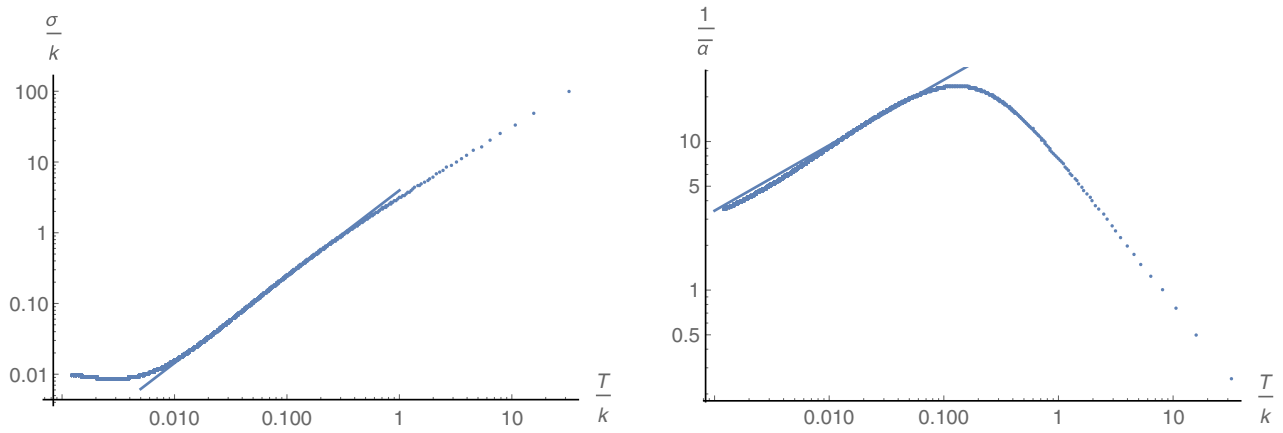

FIG. 7. Plot for the conductivities σ and $\bar{\alpha}$ as functions of the reduced temperature T/k for a family of solutions with fixed $\mu/k = 0.01$. The straight lines correspond to fits in the intermediate scaling regime.

and from this, we can compute the conductivities σ and $\bar{\alpha}$ as

$$\sigma = \frac{\partial J}{\partial E} = \frac{2a_{t_1}^2 h_0^6 r_h^3}{f_0^2 k^2} + \frac{r_h}{h_0^2},$$
$$\bar{\alpha} = \frac{1}{T}\frac{\partial Q}{\partial E} = \frac{4\pi a_{t_1} h_0^6 r_h^3}{f_0 k^2}. \tag{38}$$

In Fig. 7, we show these conductivities for the family of solutions presented in Fig. 6. From the plot, we see that the conductivities show that at high temperatures we have that $\sigma \sim \bar{\alpha} \sim T/k$, which agrees with the expectations for a CFT_4. In the low-temperature regime, we have $\sigma \sim 0.22$ and $\bar{\alpha} \sim 0.44$. Interestingly, form intermediate temperatures, we see that the conductivities develop a power law scaling, $\sigma \sim (T/k)^{1.38}$ and $\bar{\alpha} \sim (T/k)^{-0.44}$. Another interesting feature of the conductivity σ is that it is not monotonous with the temperature, giving a metallic behavior at low T/k and an insulator one at high temperatures [24].

Now, to compute the remaining conductivities, we perturb the Einstein-Maxwell solutions as

$$\delta A = (-t\delta f_1(r) + \delta a_x(r))dx,$$
$$\delta ds^2 = (t\delta f(r) + h_{tx}(r))dxdt + h_{rx}dxdr. \tag{39}$$

Following as in the previous section, we obtain expressions for J and Q that do not depend on the radial direction and can be just expressed as a function of IR data,

$$J = \frac{r_h\left(\frac{2a_{t_1}h_0^8 r_h^2(\zeta r_h(a_{t_1}^2 - 12f_0^2) + 6a_{t_1}E)}{f_0^2 k^2} + a_{t_1}\zeta r_h + 6E\right)}{6h_0^2},$$
$$Q = -\frac{r_h(2h_0^8 r_h^2(a_{t_1}^2 - 12f_0^2) + f_0^2 k^2)(2h_0^8 r_h(\zeta r_h(a_{t_1}^2 - 12f_0^2) + 6a_{t_1}E) + \zeta f_0^2 k^2)}{72 f_0^2 h_0^{10} k^2}, \tag{40}$$

where we erased the temporal dependence, fixing

$$\delta f_1(r) = E + \zeta A_t(r),$$
$$\delta f(r) = 2\zeta r^2 f(r)^2 g(r), \tag{41}$$

and we use that

$$\delta h_{rx} = -\frac{2rh^8 A_t'(\zeta r A_t' + 6\zeta A_t + 6E) + \zeta f^2(12r^2h^6(-r^2gh'^2 + rghh' + 2(g-1)h^2) + k^2)}{3k^2 r f^2 g}, \tag{42}$$

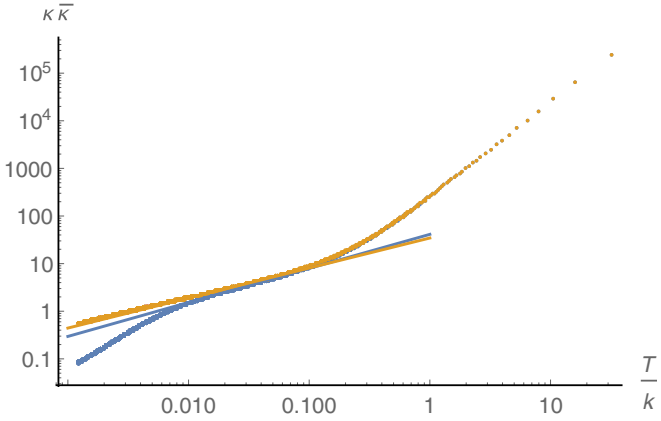

FIG. 8. Conductivities $\bar{\kappa}$ (blue) and κ (orange) as functions of the reduced temperature T/k for a family of solutions with fixed $\mu/k = 0.01$.

Then, the remaining transport coefficients read

$$\alpha = \frac{4\pi a_{t_1} h_0^6 r_h^3}{f_0 k^2},$$
$$\bar{\kappa} = -\frac{\pi r_h^2 \left(\frac{2h_0^8 r_h^2 (a_{t_1}^2 - 12 f_0^2)}{k^2} + f_0^2\right)}{3 f_0 h_0^2}. \tag{43}$$

Again, we obtain the expected result $\alpha = \bar{\alpha}$. The thermal conductivity at zero electric current is written in this case as

$$\kappa = \bar{\kappa} - \frac{\alpha\bar{\alpha}T}{\sigma} = -\frac{2\pi f_0 h_0^8 r_h^4 (a_{t_1}^2 - 12 f_0^2) + \pi f_0^3 k^2 r_h^2}{3 h_0^2 (2 a_{t_1}^2 h_0^8 r_h^2 + f_0^2 k^2)}. \tag{44}$$

In the left panel of Fig. 8, we plot the thermal conductivities κ and $\bar{\kappa}$ for a family of black holes at fixed chemical potential $\mu/k = 0.01$. For large temperatures, we see that $\bar{\kappa} \sim (T/k)^2$. For low temperatures, we have that $\bar{\kappa} \sim 0.54$, while $\kappa \sim (T/k)^{1.45}$. In the intermediate regime, we find that $\bar{\kappa} \sim (T/k)^{0.63}$, while $\kappa \sim (T/k)^{0.71}$. Again, the qualitative difference between κ and $\bar{\kappa}$ signals the break of the quasiparticle picture at low enough temperatures.

IV. $SL_2(\mathcal{R})$ BLACK HOLES WITH INTERMEDIATE SCALING

Finally, let us consider black brane solutions corresponding to foliations of an $SL_2(\mathcal{R})$ metric.

A. Solutions

We will work with the ansatz

$$A = A_t(r) dt,$$
$$ds^2 = -r^2 g(r) f(r)^2 dt^2 + \frac{1}{r^2 g(r)} dr^2 + \frac{r^2 h^2(r)}{k^2 x^2}(dx^2 + dy^2) + \frac{r^2}{h^4(r)}\left(dz + \frac{dy}{kx}\right)^2. \tag{45}$$

The equations of motion read

$$\frac{2r^2\left(\frac{A_t'^2}{f^2} - 12\right) + 12 g\left(\frac{r^2 h'^2}{h^2} + 1\right) + \frac{(4h^6+1)}{k^2 h^8}}{6r} + g' = 0,$$
$$h'' - \frac{2r^3 h^8 A_t'^2 h' + 6r^4 f^2 g h^7 h'^2 - 6r^3 f^2 g h^8 h' + 4k^2 r f^2 h^6 h' + k^2 r f^2 h' - 24 r^3 f^2 h^8 h' - 2k^2 f^2 h^7 - 2k^2 f^2 h}{6 r^4 f^2 g h^8} = 0,$$
$$f' - \frac{2 r f h'^2}{h^2} = 0, \qquad A_t'' - \frac{A_t'(r f' - 3f)}{r f} = 0. \tag{46}$$

We will numerically integrate these equations from the near horizon,

$$A_t(r) \simeq a_{t_1}(r - r_h) - \frac{1}{2} a_{t_1}\left(3 - \frac{f_1}{f_0}\right)(r - r_h)^2 + \ldots,$$
$$f(r) \simeq f_0 + \frac{8 f_0^5 (h_0^6 + 1)^2 k^4}{r_h (2 h_0^8 r_h^2 (a_{t_1}^2 - 12 f_0^2) + f_0^2 (4 h_0^6 + 1) k^2)^2}(r - r_h) + \ldots,$$
$$g(r) \simeq \left(\frac{r_h^2 (24 - \frac{2 a_{t_1}^2}{f_0^2}) - \frac{(4h_0^6+1)k^2}{h_0^8}}{6 r_h^3}\right)(r - r_h) + \ldots,$$
$$h(r) \simeq h_0 + \frac{2 f_0^2 h_0 (h_0^6 + 1) k^2}{2 h_0^8 r_h^3 (a_{t_1}^2 - 12 f_0^2) + f_0^2 (4 h_0^6 + 1) k^2 r_h}(r - r_h) + \ldots, \tag{47}$$

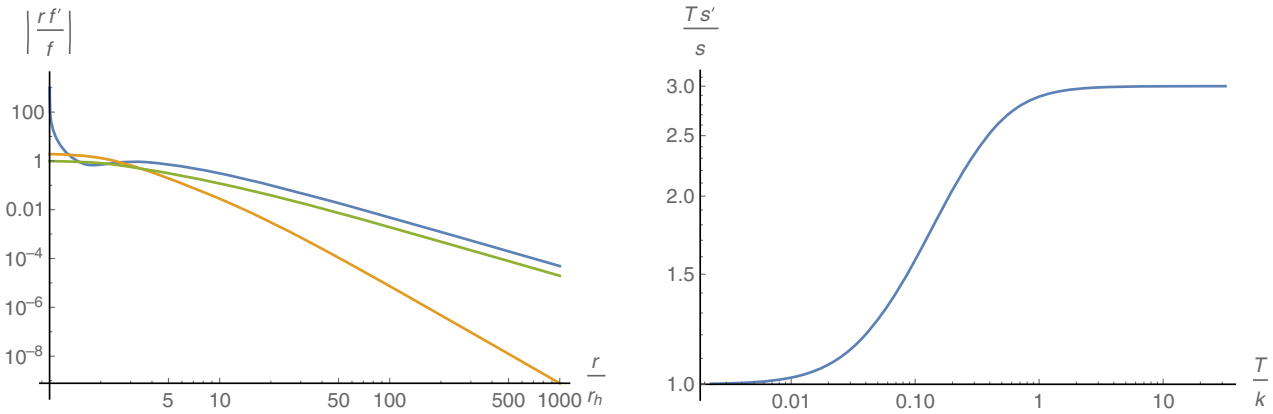

FIG. 9. Left: Typical profile for $f(r)$ (blue), $g(r)$ (orange), and $h(r)$ (green). The combination rf'/f, where f corresponds to any of the aforementioned functions, was chosen to make manifest the emergence of new scalings towards the IR. The plot corresponds to a solution with $T/k = 0.00225$ and $\mu/k = 0$. Right: Ts'/s as a function of the reduced temperature T/k.

towards the boundary

$$A_t(r) \simeq \mu + \frac{\rho}{r^2} - \frac{\rho(1+h_\infty^6)^2k^4}{216h_\infty^{16}r^6} + \ldots,$$
$$f(r) \simeq f_\infty - \frac{f_\infty(1+h_\infty^6)^2k^4}{72h_\infty^{16}r^4} + \ldots,$$
$$g(r) \simeq 1 - \frac{(1+4h_\infty^6)k^2}{12h_\infty^8r^2} + \frac{g_4^\infty}{r^4} + \frac{(1+h_\infty^6)^2k^4\log r}{18h_\infty^{16}r^4} + \ldots,$$
$$h(r) \simeq h_\infty + \frac{(1+h_\infty^6)k^2}{12h_\infty^7r^2} + \frac{h_4^\infty}{r^4} + \ldots, \tag{48}$$

through a shooting method. A typical solution is shown in Fig. 9.

The black hole thermodynamics is dictated by

$$T = \frac{f_0\left(r_h^2\left(24 - \frac{2a_{t_1}^2}{f_0^2}\right) - \frac{(4h_0^6+1)k^2}{h_0^8}\right)}{24\pi r_h},$$
$$s = 2\pi r_h^3. \tag{49}$$

We are now ready to construct a family of solutions that is characterized by the parameter T/k and μ/k. Again, we first look for solutions with $\mu = 0$, and we find that for low enough T/k the metric profiles develop a scaling in the deep IR near the black hole horizon. This scaling is shown in Fig. 9, in which we see for a particular solution that near the horizon $f \sim (r/r_h)^2$ and $h \sim (r/r_h)^{-1}$. This implies that the dual field theory will have an IR scaling dictated by

$$t \to \lambda^1 t, \quad \omega_1 \to \omega_1, \quad \omega_2 \to \omega_2, \quad \omega_3 \to \lambda^1\omega_3. \tag{50}$$

This scaling is also reflected in the fact that the entropy scales as $s/k^3 \sim T/k$ at low temperatures.

When we turn on the chemical potential, the IR scalings become intermediate scalings, and the near-horizon geometry becomes $\mathrm{AdS}_2 \times SL_2(\mathcal{R})$. A typical family of solutions and a typical profile is shown in Fig. 10. In the following subsection, we will use this family of solutions to study the dc transport properties of the dual field theory.

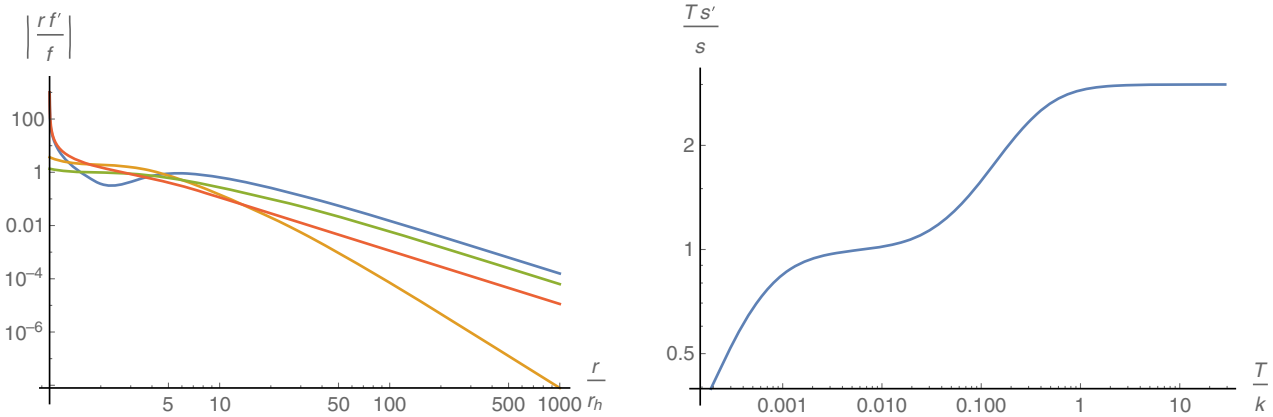

FIG. 10. Left: Typical profile for $f(r)$ (blue), $g(r)$ (orange), $h(r)$ (green), and $A_t(r)$ (red). The combination rf'/f, where f corresponds to any of the aforementioned functions, was chosen to make manifest the emergence of new scalings towards the IR. The plot corresponds to a solution with $T/k = 0.0001892$ and $\mu/k = 0.01$. Right: Ts'/s as a function of the reduced temperature T/k.

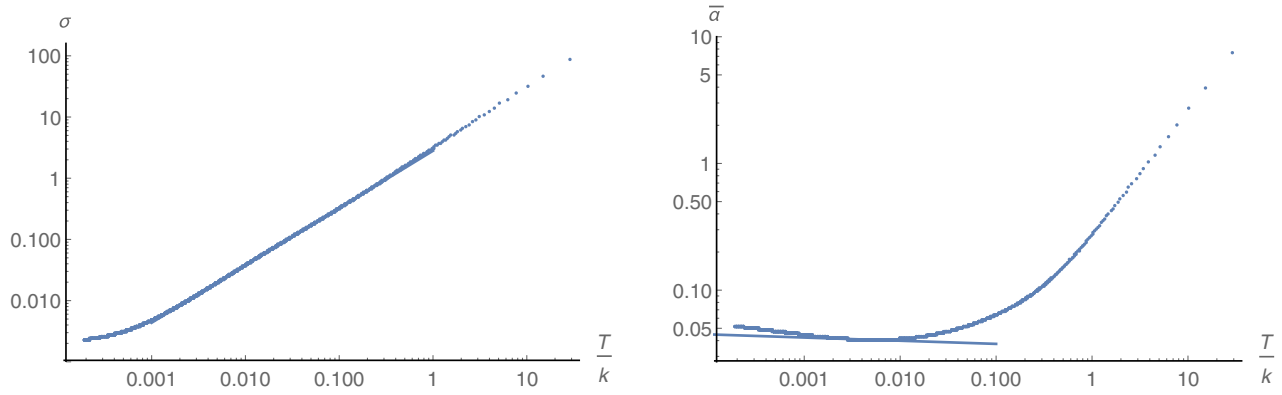

FIG. 11. Plot for the conductivities σ and $\bar{\alpha}$ as functions of the reduced temperature T/k for a family of solutions with fixed $\mu/k = 0.01$. The straight lines correspond to fits in the intermediate scaling regime.

B. Computing the transport coefficients

Let us start with the fluctuations along the x direction,

$$\begin{aligned}\delta A &= (-Et + \delta a_x(r))dx \\ \delta ds^2 &= h_{tx}(r)dtdx + h_{rx}(r)drdx,\end{aligned} \tag{51}$$

with E being the constant electric field. From the Einstein and Maxwell equations, we obtain the conserved current and charge J and Q, and the remaining equation for h_{rx} reads

$$h_{rx} = -\frac{4Eh^8A_t'}{k^2f^2g(2h^6+1)}. \tag{52}$$

Using the near-horizon data (47) and asking for regularity, we have that the conserved quantities read

$$\begin{aligned}J &= \frac{2a_{t_1}^2h_0^6r_h^3E}{f_0^2(2h_0^6+1)k^2} + \frac{r_hE}{h_0^2}, \\ Q &= \frac{a_{t_1}h_0^6r_h^2E\left(r_h^2\left(24-\frac{2a_{t_1}^2}{f_0^2}\right)-\frac{(4h_0^6+1)k^2}{h_0^8}\right)}{6(2h_0^6+1)k^2}.\end{aligned} \tag{53}$$

From this, we compute the conductivities σ and $\bar{\alpha}$, which have the following expression:

$$\begin{aligned}\sigma &= \frac{\partial J}{\partial E} = \frac{2a_{t_1}^2h_0^6r_h^3}{f_0^2(2h_0^6+1)k^2} + \frac{r_h}{h_0^2}, \\ \bar{\alpha} &= \frac{1}{T}\frac{\partial Q}{\partial E} = \frac{4\pi a_{t_1}h_0^6r_h^3}{k^2(2f_0h_0^6+f_0)}.\end{aligned} \tag{54}$$

In Fig. 11, we plot these coefficients for the family of solutions presented in Fig. 10. From the plot, we see that at large temperatures the coefficients scale as $\sigma/k \sim \bar{\alpha} \sim T/k$. This is again the expected result for CFT_4. As we lower the temperature, we find that in the intermediate scaling regime the conductivities also follow power laws. For σ/k, we observe that still goes linearly with the reduced temperature, while $\bar{\alpha}$ remains constant. In the low-temperature regime, we find $\sigma/k \sim (T/k)^{1/4}$ and $\bar{\alpha} \sim 0.052$.

Now, let us continue with the computation of the remaining conductivities. To do that, we perturb the Einstein-Maxwell solutions shown in Fig. 10 by

$$\begin{aligned}\delta A &= (-t\delta f_1(r) + \delta a_x(r))dx, \\ \delta ds^2 &= (t\delta f(r) + h_{tx}(r))dxdt + h_{rx}dxdr.\end{aligned} \tag{55}$$

Following as in the previous sections, we obtain expressions for J and Q that do not depend on the radial direction and can be just expressed as a function of IR data,

$$\begin{aligned}J &= \frac{f_0^2k^2r_h(6(2h_0^6+1)E - a_{t_1}\zeta(4h_0^6+1)r_h) - 2a_{t_1}h_0^8r_h^3(\zeta r_h(a_{t_1}^2-12f_0^2)+6a_{t_1}E)}{6f_0^2h_0^2(2h_0^6+1)k^2}, \\ Q &= \frac{r_h(2h_0^8r_h^2(a_{t_1}^2-12f_0^2)+f_0^2(4h_0^6+1)k^2)(2h_0^8r_h(\zeta r_h(a_{t_1}^2-12f_0^2)+6a_{t_1}E)+\zeta f_0^2(4h_0^6+1)k^2)}{72f_0^2h_0^{10}(2h_0^6+1)k^2},\end{aligned} \tag{56}$$

where we erased the temporal dependence, fixing

$$\begin{aligned}\delta f_1(r) &= E + \zeta A_t, \\ \delta f(r) &= 2r^2\zeta f^2 g,\end{aligned} \tag{57}$$

and we used that one of the Einstein equations is

$$\delta h_{rx} = -\frac{2k^2rh^8A_t'(\zeta rA_t' + 6\zeta A_t + 6E) + \zeta f^2(12r^2h^6(-r^2gh'^2 + rghh' + 2(g-1)h^2) + \frac{1}{k^2})}{3rf^2g}. \tag{58}$$

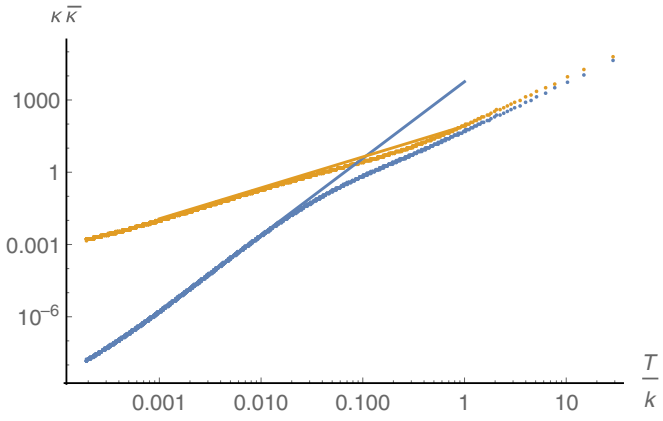

FIG. 12. Conductivities $\bar{\kappa}$ (blue) and κ (orange) as functions of the reduced temperature T/k for a family of solutions with fixed $\mu/k = 0.01$.

Then, the remaining transport coefficients read

$$\alpha = \frac{4\pi a_{t_1} h_0^6 r_h^3}{k^2(2f_0 h_0^6 + f_0)},$$
$$\bar{\kappa} = \frac{\pi r_h^2(-2h_0^8 r_h^2(a_{t_1}^2 - 12f_0^2) - f_0^2(4h_0^6+1)k^2)}{3h_0^2 k^2(2f_0 h_0^6 + f_0)}. \quad (59)$$

We recover the expected result $\alpha = \bar{\alpha}$. The thermal conductivity at zero electric current is written for this gravity solution as

$$\kappa = \bar{\kappa} - \frac{\alpha\bar{\alpha}T}{\sigma} = \frac{2\pi f_0 h_0^8 r_h^4(12f_0^2 - a_{t_1}^2) - \pi f_0^3(4h_0^6+1)k^2 r_h^2}{6a_{t_1}^2 h_0^{10} r_h^2 + 3f_0^2(2h_0^6+1)h_0^2 k^2}. \quad (60)$$

In Fig. 12, we compare these two quantities and their behavior as functions of the reduced temperature. Again, we recover the expected $\kappa \sim \bar{\kappa} \sim (T/k)^2$ at high temperatures. As we lower the temperature and enter into the intermediate regime, we see that κ and $\bar{\kappa}$ start to scale differently, $\kappa \sim (T/k)^{3.19}$ and $\kappa \sim (T/k)^{1.28}$. In the low-temperature regime, we find $\kappa \sim (T/k)^{2.53}$ and $\kappa \sim (T/k)^{0.97}$.

V. SUMMARY AND FUTURE DIRECTIONS

We constructed a class of black holes that implements a RG flow which passes through intermediate scaling solutions within Einstein-Maxwell-AdS theory. These intermediate scalings are anisotropic and are triggered by the fact that the theory lives in a curved geometry associated to a Bianchi geometry (1). An interesting characteristic of our solutions is that in the intermediate regime different spatial directions scale differently, giving a generalized idea of Lifshitz scaling. We summarize the scalings of the spacetime for charged solutions in the Table I.

In the lattice induced scalings presented in Refs. [2,15,16], all spatial directions have the same scalings. We believe that this might be a consequence of considering square lattices, and it would be nice to check if different lattice shapes will induce anisotropic scalings like the ones we present here.

The dc conductivities also reflect the fact that there exist new scaling solutions at intermediate temperatures. In the following Table II, we summarize the powers of T/k obtained for the different conductivities and black hole solutions.

Let us finish by discussing some possible future directions. A first direction would be to check the generality of our results by studying other possible boundary geometries. In Ref. [14], the authors studied the Einstein equations with a Bianchi VII_0 deformation and found boomerang RG flows. It would be interesting to see wether one can find also intermediate scalings in the large helical deformation regime. Another promising geometry to explore would be the squashed sphere Bianchi type IX.

TABLE I. Scalings for the invariant one forms in the different energy scales.

	t			ω_1			ω_2			ω_3		
	UV	Inter.	IR	UV	Inter.	IR	UV	Inter.	IR	UV	Inter.	IR
Solv	1	1	1	1	0	0	1	1	0	1	0	0
Nil	1	11/8	1	1	1	0	1	1	0	1	3/2	0
$SL_2(\mathcal{R})$	1	1	1	1	0	0	1	0	0	1	1	0

TABLE II. Scalings for the transport coefficients in the different energy scales.

	σ/k			α			κ			$\bar{\kappa}$		
	UV	Intermediate	IR	UV	Intermediate	IR	UV	Intermediate	IR	UV	Intermediate	IR
Solv	1	1.88	0.14	1	0.39	0	2	1.66	1.5	2	1.66	1
Nil	1	1.38	0	1	−0.44	0	2	0.71	1.45	2	0.63	0.65
$SL_2(\mathcal{R})$	1	1	0.25	1	0	0	2	3.19	2.53	2	1.28	0.97

Another interesting direction would be to explore the effect of $U(1)$ symmetry breaking in the scalings. In this direction, a holographic superconductor living on an helical background was studied in Ref. [25]. There, the helix is supported by a Proca field. It would be an interesting exercise to repeat their study within the simpler Einstein-Maxwell context.

Finally, it would be interesting to see how these scalings appear in the weak coupling limit by studying a theory with simple field content living in one of the spaces studied above. It would be nice to find in some toy model how the anisotropic scalings appear in perturbation theory.

ACKNOWLEDGMENTS

We would like to thank Gonzalo Torroba for insightful discussions. I. S. L. acknowledges hospitality from IFLP, where part of this work was done.

[1] G. T. Horowitz, J. E. Santos, and D. Tong, Optical conductivity with holographic lattices, J. High Energy Phys. 07 (2012) 168.
[2] G. T. Horowitz, J. E. Santos, and D. Tong, Further evidence for lattice-induced scaling, J. High Energy Phys. 11 (2012) 102.
[3] G. T. Horowitz and J. E. Santos, General relativity and the cuprates, J. High Energy Phys. 06 (2013) 087.
[4] D. Vegh, Holography without translational symmetry, arXiv:1301.0537.
[5] M. Blake and D. Tong, Universal resistivity from holographic massive gravity, Phys. Rev. D **88**, 106004 (2013).
[6] M. Blake, D. Tong, and D. Vegh, Holographic Lattices give the Graviton an Effective Mass, Phys. Rev. Lett. **112**, 071602 (2014).
[7] A. Amoretti, A. Braggio, N. Maggiore, N. Magnoli, and D. Musso, Thermo-electric transport in gauge/gravity models with momentum dissipation, J. High Energy Phys. 09 (2014) 160.
[8] A. Amoretti, A. Braggio, N. Maggiore, N. Magnoli, and D. Musso, Analytic dc thermoelectric conductivities in holography with massive gravitons, Phys. Rev. D **91**, 025002 (2015).
[9] A. Donos and S. A. Hartnoll, Interaction-driven localization in holography, Nat. Phys. **9**, 649 (2013).
[10] N. Iizuka, S. Kachru, N. Kundu, P. Narayan, N. Sircar, and S. P. Trivedi, Bianchi attractors: A classification of extremal black brane geometries, J. High Energy Phys. 07 (2012) 193.
[11] C. Cadeau and E. Woolgar, New five-dimensional black holes classified by horizon geometry, and a Bianchi VI brane world, Classical Quantum Gravity 18 (**2001**) 527.
[12] M. Hassaine, New black holes of vacuum Einstein equations with hyperscaling violation and Nil geometry horizons, Phys. Rev. D **91**, 084054 (2015).
[13] R. E. Arias and I. Salazar Landea, Thermoelectric transport coefficients from charged Solv and Nil black holes, J. High Energy Phys. 12 (2017) 087.
[14] A. Donos, J. P. Gauntlett, and C. Pantelidou, Conformal field theories in $d = 4$ with a helical twist, Phys. Rev. D **91**, 066003 (2015).
[15] A. Donos, J. P. Gauntlett, C. Rosen, and O. Sosa-Rodriguez, Boomerang RG flows in M-theory with intermediate scaling, J. High Energy Phys. 07 (2017) 128.
[16] A. Donos, J. P. Gauntlett, C. Rosen, and O. Sosa-Rodriguez, Boomerang RG flows with intermediate conformal invariance, J. High Energy Phys. 04 (2018) 017.
[17] S. A. Hartnoll and A. Karch, Scaling theory of the cuprate strange metals, Phys. Rev. B **91**, 155126 (2015).
[18] A. Donos and J. P. Gauntlett, Thermoelectric DC conductivities from black hole horizons, J. High Energy Phys. 11 (2014) 081.
[19] J. Bhattacharya, S. Cremonini, and B. Goutraux, Intermediate scalings in holographic RG flows and conductivities, J. High Energy Phys. 02 (2015) 035.
[20] H. S. Liu, H. Lu, and C. N. Pope, Holographic heat current as Noether current, J. High Energy Phys. 09 (2017) 146.
[21] A. Donos, J. P. Gauntlett, T. Griffin, and L. Melgar, DC conductivity and higher derivative gravity, Classical Quantum Gravity **34**, 135015 (2017).
[22] R. Mahajan, M. Barkeshli, and S. A. Hartnoll, Non-Fermi liquids and the Wiedemann-Franz law, Phys. Rev. B **88**, 125107 (2013).
[23] A. Donos, B. Gouteraux, and E. Kiritsis, Holographic metals and insulators with helical symmetry, J. High Energy Phys. 09 (2014) 038.
[24] M. Baggioli and M. Goykhman, Phases of holographic superconductors with broken translational symmetry, J. High Energy Phys. 07 (2015) 035.
[25] J. Erdmenger, B. Herwerth, S. Klug, R. Meyer, and K. Schalm, S-Wave superconductivity in anisotropic holographic insulators, J. High Energy Phys. 05 (2015) 094.